

Photospheric signatures imprinted on the γ -ray burst spectra

Enrico Ramirez-Ruiz¹

School of Natural Sciences, Institute for Advanced Study, Einstein Drive, Princeton, NJ 08540, USA.

¹*Chandra Fellow.*

ABSTRACT

A solution is presented for the spectrum of high-energy GRB photons confined to a quasi-thermal baryonic photosphere. The solution is valid in the steady-state limit assuming the region under consideration is optically thick to the continuously injected photons. It is shown that for a high luminosity photosphere, the non-thermal electrons resulting from γ -ray Compton cooling lose their energy by upscattering the soft thermalised radiation. The resulting spectral modifications offer the possibility of diagnosing not only the burst comoving luminosity but also the baryon load of the ejecta. This model leads to a simple physical interpretation of X-ray rich bursts and anomalous low-energy slopes.

Key words: gamma rays: theory – radiation mechanisms:non-thermal

1 INTRODUCTION

A quasi-thermal photosphere is expected in all GRB ejecta (Cavallo & Rees 1978; Goodman 1986; Shemi & Piran 1990), either due to pairs or to baryonic electrons, in addition to a possible non-thermal component from dissipation (shocks or reconnection). Preponderance of one or the other depends on whether the photosphere occurs inside or outside the saturation radius where the bulk Lorentz factor saturates to the dimensionless entropy of the outflow. Below the saturation radius, the photospheric luminosity dominates whereas above it the greater part of the energy is in kinetic form. In the latter case, the energy available in the form of radiation or pairs depends on the variable portion of the outflow and the efficiency of dissipation in shocks (Daigne & Mochkovitch 2002; Ramirez-Ruiz et al. 2002), or on the reconnection efficiency (Mészáros & Rees 2000).

In this Letter we investigate the relationship between the quasi-thermal baryon-related photosphere in relativistic outflows, and the internal shock arising around this limiting radius. This photosphere is a source of soft thermal radiation, which may be observationally detectable in some GRB spectra (Murakami et al. 1991). In these models, dissipation happens whenever internal shocks develop in the ejecta (Rees & Mészáros 1994), which reconverts some fraction of the kinetic energy into radiation. If this dissipation takes place below the photosphere, the non-thermal shock luminosity could compensate for the adiabatic decrease of the post-saturation photospheric luminosity, so that the radiative efficiency in the outflow would be high. The relative roles of photosphere and shocks are reexamined in Section 2. A solution is presented in Section 3 for the spectrum of high energy γ -rays confined to a quasi-thermal baryonic photosphere and the possible non thermal spectral distortions in it. The relation of these ideas to GRB phenomenology is outlined in Section 4.

2 PHOTOSPHERES AND SHOCKS

Consider a relativistic wind outflow expanding from some initial minimum radius $r_0 = c\delta t = 10^7 r_{0,7}$ cm, where the wind baryon load \dot{M} is parametrized by a dimensionless entropy $\eta = L_0/\dot{M}c^2$. We then assume that the actual value of η (or L_0) is unsteady. The Lorentz factor saturates to $\Gamma \sim \eta$ at a saturation radius $r_\eta/r_0 \sim \eta$ where the wind energy density, in radiation or in magnetic energy, drops below the baryon rest mass density in the comoving frame (Shemi & Piran 1990). The location of the baryonic photosphere, where $\tau_T = 1$, due to electrons associated with baryons, is

$$r_\tau = \frac{\dot{M}\sigma_T}{4\pi m_p c \Gamma^2} \approx 10^{13} L_{0,52} \eta_2^{-3} \text{ cm}, \quad (1)$$

where $\eta_2 = \eta/10^2$ and $L_{0,52} = L_0/10^{52}$ erg. The above equation holds provided that η is low enough that the wind has already reached its terminal Lorentz factor at r_τ . This requires (Mészáros & Rees 2000)

$$\eta \leq \eta_* = \left(\frac{L_0 \sigma_T}{4\pi m_p c^3 r_0} \right)^{1/4} \simeq 10^3 L_{0,52}^{1/4} r_{0,7}^{-1/4}. \quad (2)$$

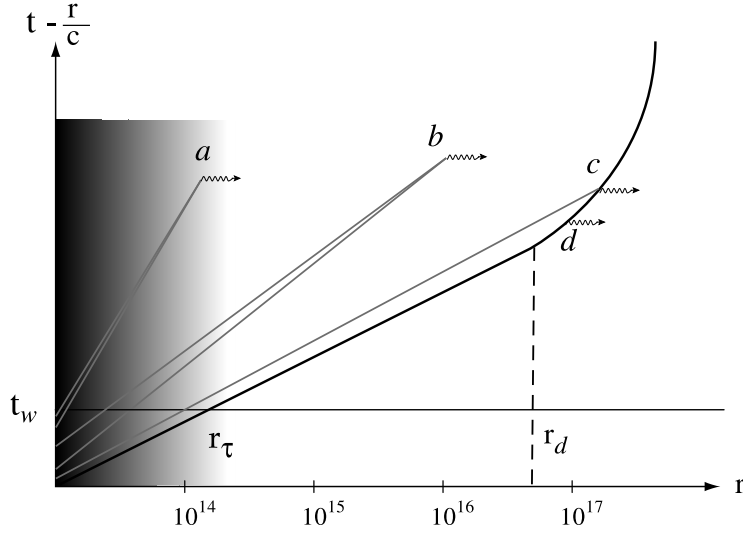


Figure 1. Schematic spacetime diagram in source frame coordinates of a relativistic outflow. The axes (logarithmic) are r versus $t - (r/c)$, where t is time measured by a distant observer, and is zero when the burst is observed to start. In this plot, light rays are horizontal lines. The primary gamma-ray emission is assumed to continue, with a quasi-steady luminosity L_w , for a time t_w . If Γ fluctuates by a factor of ~ 2 around its mean value, relative motions within the outflowing material give rise to internal shocks. Decreasing η values lead to world lines further to the left. In case (a), $\eta < \eta_\tau$ and the dissipation occurs when the wind is optically thick. In case (b), with $\eta_d > \eta > \eta_\tau$, ejecta collide in an optically thin region before reaching the contact discontinuity. The contact discontinuity and the forward shock are being decelerated because of the increasing amount of external matter being swept up (giving rise to a long-term afterglow; case [d]), so that they lag behind the light cone by an increasing amount Δr , whose increase with r is steeper than linear. This deceleration allows ejecta to catch up and pass through a reverse shock just inside the contact discontinuity (case [c]).

If the value of η at the base increases by a factor ≥ 2 over a timescale δt , then the later ejecta will catch up and dissipate a significant fraction of their energy at some radius $r_\iota > r_\eta$ given by

$$r_\iota \sim c\delta t\eta^2 \sim 3 \times 10^{14} \delta t_0 \eta_2^2 \text{ cm.} \quad (3)$$

The shocks cannot occur when $r < r_\eta$ since in this region both shells accelerate at the same rate $\Gamma \propto r$ and do not catch up. In order for a shock to occur above a photosphere which is in the coasting region

$$\eta \geq \eta_\tau \approx 50 L_{0,52}^{1/5} \delta t_0^{-1/5}, \quad (4)$$

if one takes $r_0 \sim c\delta t$, where $\delta t_0 = \delta t/1$ sec. If, on the other hand, $\delta t \sim 10^{-3}$ sec, then $\eta_\tau \sim 200$.

The initial wind starts to decelerate when it has swept up $\sim \eta^{-1}$ of its initial mass. For sufficiently high η , the deceleration radius can formally become smaller than the collisional radius of equation (3). This requires

$$\eta \geq \eta_d \approx 8 \times 10^2 L_{0,52}^{1/8} t_w^{1/8} n_0^{-1/8} \delta t_0^{-3/8}. \quad (5)$$

This deceleration allows slower ejecta to catch up, replenishing and re-energising the reverse shock and boosting the momentum in the blast wave.

Fig. 1 shows the schematic world-lines of a relativistic outflow with a range of Lorentz factors. We identify three types of contributions to the observed time history, each with a different character. For a relatively low Lorentz factor $\eta < \eta_\tau$, as in curve (a) of Fig. 1, the radius $r_\iota < r_\tau$, and the dissipation occurs before the wind is optically thin. Below the baryonic photosphere, shocks would occur at high optical depths. Section 3 investigates the relationship between the quasi-thermal baryon-related photosphere in relativistic outflows and the internal shocks arising near this limiting region. For a larger Lorentz factor $\eta > \eta_d$, corresponding to curve (c) of Fig. 1, the ejecta would expand freely until the contact discontinuity had been decelerated by sweeping up external material. It would then crash into the reverse shock, thermalising its energy and boosting the power of the afterglow. The impact of such collisions on the prompt emission have been studied in Ramirez-Ruiz, Merloni & Rees (2001). In curve (b), with intermediate η , deceleration occurs at radii $r_d > r_\iota$, and dissipation takes place when the wind is optically thin (i.e. when it is most effective).

2.1 Photospheric and Internal Shock Luminosity

The lab-frame baryonic photospheric luminosity L_τ and dimensionless temperature Θ_τ evolve as $(L_\tau/L_0) = (\Theta_\tau/\Theta_0) = (r_\tau/r_\eta)^{-2/3}$, where $\Theta_0 = kT_0/m_e c^2 \simeq 2L_{0,52}^{1/4} r_{0,7}^{-1/2}$ is the initial temperature at r_0 . Using the expression for r_τ , this can be written as $(L_\tau/L_0) = (\eta/\eta_*)^{8/3}$ for $\eta < \eta_*$ and 1 otherwise.

The internal shocks in the wind can dissipate a fraction of the terminal kinetic energy luminosity L_0 above the saturation radius r_η , $L_\iota = \epsilon_\epsilon \epsilon_\iota L_0 \sim 10^{-1} (3\epsilon_\epsilon) (3\epsilon_\iota) L_0$, where $\epsilon_\epsilon \epsilon_\iota$ is a bolometric radiative efficiency when the cooling timescale is shorter than the dynamical

time. If the Poynting flux provides a fraction α of the total luminosity L_0 at the base of the wind (at r_0), the magnetic field there is $B_0 \sim 10^{10} \alpha^{1/2} L_{0,51}^{1/2} \delta t_0^{-1}$ G. The comoving magnetic field at r_ι is $B_\iota = B_0 (r_0/r_\eta)^2 (r_\eta/r_\iota) \sim 10^4 \alpha^{1/2} L_{w,51}^{1/2} \delta t_0^{-1} \eta_2^{-3}$ G. If the electrons are accelerated in the dissipation shocks to a Lorentz factor $\gamma = 10^3 \gamma_3$, the ratio of the synchrotron cooling time to the dynamic expansion time in the comoving frame is $(t_{\text{sy}}/t_{\text{adi}})_\iota \sim 5 \times 10^{-3} \alpha^{-1} L_{0,51}^{-1} \gamma_3^{-1} \delta t_0 \eta_2^5$ so a very high radiative efficiency is ensured even for δt as high as seconds. It is therefore clear that a magnetic field can ensure efficient cooling even if it is not strong enough to be dynamically significant (i.e. even for $\alpha \ll 1$).

For a given L_0 , an individual burst is characterized by an average η . For $\eta > \eta_*$, the photosphere arises in the accelerating region, and in this region shocks are not possible. For $\eta_\tau < \eta < \eta_*$, we have $L_\tau > L_\iota$, so that the baryonic photospheric component dominates the non-thermal internal shock component in a bolometric sense. Low values of η lead to further out, weaker photospheres and, at the same time, relative stronger shocks occurring near the photosphere. For $L_\tau \leq L_\iota$, the thermal photospheric peak will tend to blend with the synchrotron peak, resembling the canonical non thermal GRB spectrum. For lower $\eta < \eta_\tau$, the thermal peak is even softer with $L_\tau \ll L_\iota$, while shocks occur closer in and produce harder synchrotron peaks (Ramirez-Ruiz & Lloyd-Ronning 2002). The corresponding shocks occur below (or near) the baryonic photosphere where the scattering depth of the shells is larger (Panaitescu et al. 1999; Ramirez-Ruiz & Lloyd-Ronning 2002, Kobayashi et al. 2002). Shocks which occur inside the photosphere may also induce Alfvén waves and these waves can be efficiently damped for $r < r_\tau$ (i.e. $\tau_T > 1$).

3 THE EFFECTS OF A REPROCESSING PHOTOSPHERE ON THE GRB SPECTRA

We consider here the problem of Compton downscattering of X-rays and γ -rays confined to an optically thick baryonic photosphere. The electrons are assumed to have zero temperature, which is appropriate as long as the photon energies are much larger than Θ_τ . For simplicity we consider here only shocks producing a comoving spectrum with $h\nu' \leq 511$ keV so that photon-photon pair production is negligible. In this case, the pair photosphere is not sufficient to alter significantly the spectrum of the baryonic photosphere. In the following we shall assume the acceleration of electrons in the shocks to be impulsive, and therefore it has to take place in a very limited volume of the interacting shell (i.e the emitting particles do not provide an additional heating source).

We assume that GRB photons are continuously and uniformly injected at a rate $\dot{\phi}_i(\epsilon)$, where ϵ is the dimensionless photon energy in units of $m_e c^2$. For future use we take a power-law photon injection of the form $\dot{\phi}_i(\epsilon) = \Psi \epsilon^{-\beta}$, for $\epsilon \leq \epsilon_b$. Under the assumption that photosphere is optically thick, a steady photon density distribution $\phi(\epsilon)$ can be found after specifying the photon production rate and the electron density n_e of the region under consideration. This distribution is the solution to a kinetic equation where the main energy-loss mechanism is Compton scattering. $\dot{\phi}_i(\epsilon)$ satisfies an equation of the form (Arons 1971)

$$0 = \dot{\phi}_i(\epsilon) + \int_\epsilon^{\epsilon_b} d\epsilon' \phi(\epsilon') \sigma(\epsilon', \epsilon) - \phi(\epsilon) \int_{\epsilon/(1+2\epsilon)}^\epsilon d\epsilon' \sigma(\epsilon', \epsilon), \quad (6)$$

where the three terms correspond to the injection of primary photons, Compton downscattering to ϵ from higher energies, and Compton scattering out of the energy ϵ to lower energies, respectively. $\sigma(\epsilon', \epsilon)$ in equation (6) represents the probability per unit time that a photon with energy ϵ will Compton scatter from ϵ' to ϵ (Jauch & Rohrlich 1980)

$$\sigma(\epsilon', \epsilon) = \frac{3}{8} n_e c \sigma_T \left(\frac{1}{\epsilon'} \right)^2 \left[\frac{\epsilon'}{\epsilon} + \frac{\epsilon}{\epsilon'} - 2 \left(\frac{1}{\epsilon} - \frac{1}{\epsilon'} \right) + \left(\frac{1}{\epsilon} - \frac{1}{\epsilon'} \right)^2 \right]. \quad (7)$$

The integral equation (6) with the scattering rate (7) can be solved numerically by iteration for any ϵ , where the iterative steps correspond to subsequent orders of Compton scattering. In Fig. 2 are plotted representative spectra for a power-law injection of high-energy photons in the conventional coordinates ϵ and $\epsilon^2 \phi(\epsilon)$. The dotted curves give the density of the unscattered photons, ϕ_u , produced at the power law rate. The solid curves, on the other hand, give the total photon density which includes both unscattered and scattered photons. Here ϕ_u is given by $\phi_u(\epsilon) = \dot{\phi}_i(\epsilon)/[n_e \sigma(\epsilon) c]$. The calculations shown in Fig. 2 approximate the electrons in the medium to have zero temperature and assume that Compton scattering is the main interaction process for γ -rays. The results shown in Fig. 3 expand this calculation to include the role of secondary electrons (produced by Compton downscattering) under the assumption that they lose their energy mainly by upscattering the soft thermalised radiation (see Section 3.1).

The right panel of Fig. 2 shows the evolution of the photon density distribution for subsequent orders of Compton scattering. The black solid curve gives the total photon density distribution which includes both unscattered and scattered photons. The grey solid line corresponds to the density of unscattered photons, and the grey dashed curve to the sum of unscattered and singly scattered photons. The density of photons scattered once and more is therefore given by the difference between the black solid and grey dashed curves.

When $\epsilon \ll 1$, it is straightforward to present a simplified discussion of the problem. Analytical solutions are derived here largely to illustrate what may not be obvious from the numerical treatment. The last integral in equation (6) can be rewritten as

$$\int_{\epsilon/(1+2\epsilon)}^\epsilon d\epsilon' \sigma(\epsilon', \epsilon) = n_e c \sigma(\epsilon), \quad (8)$$

where $\sigma(\epsilon)$ is the Klein-Nishina cross section. In the case of $\epsilon \ll 1$, $\sigma(\epsilon) \approx \sigma_T$. The Fokker-Plank equation can then be derived by expanding (6) in powers of the small quantity $\epsilon - \epsilon'$ (Ross et al. 1978)

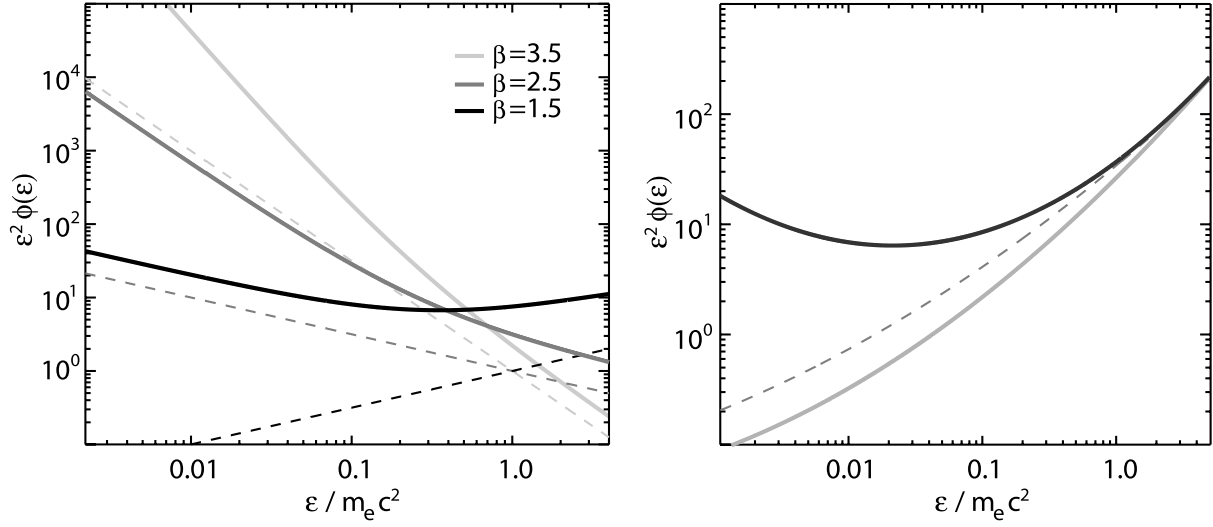


Figure 2. The photon density distribution from a power-law injection of γ -rays. The normalizations of $\phi(\epsilon)$ correspond to $\Psi/(n_e \sigma_T c) = 1$. *Left Panel:* Power-law injection of primary photons with index β and $\epsilon_b = 5$ (solid lines). The dotted curves correspond to the density of unscattered photons. *Right Panel:* The evolution of the photon density distribution in the presence of a power-law injection of primary photons with index $\beta = 1.5$ and $\epsilon_b = 10$. The black solid line gives the total photon density distribution. The grey solid line corresponds to the density of unscattered photons, and the grey dashed curve to the sum of unscattered and singly scattered photons.

$$\dot{\phi}_i = -n_e \sigma_T c \frac{d}{d\epsilon} \left[\frac{7}{10} \epsilon^6 \frac{d}{d\epsilon} \left(\frac{\phi}{\epsilon^2} \right) + \epsilon^2 \phi \right] \quad (9)$$

where the first term describes the photon energy dispersion, whereas the second characterizes the systematic changes in ϵ . Equation (9) differs from the equation of Kompaneets (1957) in that there is an additional dispersion term. For a power-law injection, the solution to equation (9) reads

$$\phi(\epsilon) \approx \frac{\Psi \epsilon^{-2}}{n_e \sigma_T c (\beta - 1)} \left[\epsilon^{1-\beta} \left(1 + \frac{7\epsilon\{\beta + 3\}}{10} \right) - \epsilon_b^{1-\beta} \left(1 + \frac{14}{5}\epsilon \right) \right]. \quad (10)$$

Here we have kept only the first two powers of ϵ . Provided that $\epsilon_b \geq 1$ and $\beta > 1$, from equation (10) it follows that $\phi/\dot{\phi}_i \propto \epsilon^{-1}$. As illustrated in Fig. 2, most of the luminosity at low energies results from γ -ray downscattering.

3.1 The role and fate of the secondary, energetic electrons

So far we have approximated the electrons in the medium to have zero temperature and have assumed that Compton scattering is the main interaction process for γ -rays. Compton cooling of γ -rays, however, produces a population of secondary energetic electrons. The fate of these electrons depends on the composition, ionization state and magnetic field present in the medium, as well as on the energy density of the background radiation. When the energy density in the (black body) photospheric photons is much larger than the energy in scattered photons (i.e. $L_\tau > L_i$), the secondary electrons will lose energy mostly in collisions with the photospheric photons and form a secondary photon spectrum. This is the situation considered in this section.

To first approximation, the scattering medium can be considered as a cold plasma if the time between successive scatterings, $t_\tau \sim \epsilon m_e c / (U_i \sigma_T)$, is much longer than the characteristic cooling time of the secondary electrons, $t_\gamma \sim \frac{3}{4} m_e c / (\gamma U_\tau \sigma_T)$. Here U_i and U_τ are the energy densities of the continuously injected photons and the photospheric radiation, respectively. The secondary electrons created by downscattering Compton cooled before the next generation of hot electrons is created if $U_\tau > \frac{3}{4} U_i / (\epsilon \gamma)$. Therefore, the bulk of the injected radiation is likely to be scattered by cooled particles when $L_\tau > L_i$. In what follows we assume the scattering medium to be ‘‘cold’’ since it greatly reduces the calculations. A detailed discussion of the relevance of a hot scattering medium, its steady state solutions for various input spectra, and its range of applicability (i.e. $L_\tau \leq L_i$) will be presented in future work.

The injected photons repeatedly downscatter to form a steady state distribution. During this process, a population of secondary, energetic electrons is injected. Down-scattering of γ -rays on a cold medium produces secondary electrons at a rate

$$\dot{n}_\gamma(\gamma) = \int_{\epsilon_m}^{\epsilon_b} d\epsilon \phi(\epsilon) \sigma(\epsilon, \epsilon - \gamma + 1), \quad (11)$$

where γ is the electron Lorentz factor and ϕ is the steady state photon density distribution. Here $\epsilon_m = \frac{1}{2}[\gamma - 1 + \{(\gamma - 1)^2 + 2(\gamma - 1)\}^{1/2}]$ is the minimum energy required for a photon to up-scatter an electron from rest to the energy γ .

The maximum energy of the secondary electrons is then given by $\gamma_b = 1 + 2\epsilon_b^2 / (1 + 2\epsilon_b)$. These secondary electrons could lose their energy mainly through synchrotron or Compton energy-loss mechanisms. One or both of these mechanisms may be present, depending on

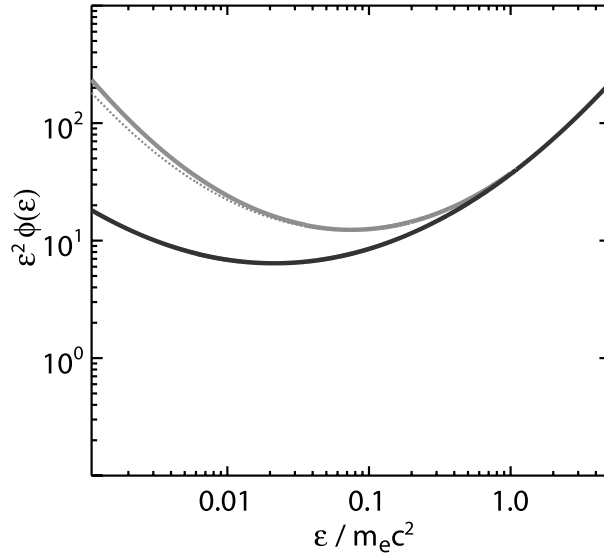


Figure 3. Illustration of the effect of Compton scattering of photospheric blackbody photons at $T_\tau = 0.5$ keV by secondary electrons. The role of secondary electrons is included under the assumption that they lose their energy mainly by upscattering the soft thermalised radiation and that they Compton cooled before the next generation of hot electrons is created. The production rate of secondary photons resulting from scatterings of the secondary energetic electrons with the black body photons is calculated and subsequently added to the total rate of photon injection. This procedure is repeated until convergence is achieved. The dark solid line gives the spectra without the effects of blackbody up-scattering (Fig. 2). The grey solid line, on the other hand, illustrates the spectral distortions arising from the inclusion of photospheric photons while the dotted line gives the photon distribution after only the first iteration procedure. The primary photons are injected with a power-law distribution with $\beta = 1.5$ and $\epsilon_b = 10$. The normalization of $\phi(\epsilon)$ correspond to $\Psi/(n_e \sigma_T c) = 1$.

the bulk Lorentz factor, the isotropic equivalent total energy of the burst, and the efficiency of dissipation in shocks. In the previous section we discussed the criteria for the non-thermal component to dominate over, or be dominated by, the photospheric thermal component. A photosphere should be prominent in the lowest baryon load cases. The black body photons can then act as seeds for scattering to higher energies, if there is substantial amount of energy in scattering centers. Alfvén waves generated by magnetic field reconnection or MHD turbulence can act as such centers. Repeated scattering on the Alfvén waves acts in the same way as Comptonisation off hot electrons.

Electrons resulting from down-scattering will therefore lose energy mostly in collisions with the photospheric emission when the energy density in the photospheric blackbody exceeds the scattered one. The steady state electron distribution (Blumenthal & Gould 1970) is given by

$$n_\gamma(\gamma) = \frac{\int_\gamma^{\gamma_b} d\gamma' \dot{n}_\gamma(\gamma')}{\frac{4}{3}\gamma^2 \sigma_T c \int_0^\infty d\epsilon_\Theta \epsilon_\Theta \phi_\Theta(\epsilon_\Theta)}, \quad (12)$$

where $\phi_\Theta(\epsilon_\Theta)$ is the blackbody photon density distribution.

The production rate of secondary high-energy photons (i.e. $\Theta > \Theta_\tau$) produced by the upscatter of blackbody photons by the secondary electrons is given by

$$\dot{\phi}_s(\epsilon) = \int_{1+\epsilon}^{\gamma_b} d\gamma n_\gamma(\gamma) \sigma_\Theta(\gamma, \gamma - \epsilon), \quad (13)$$

where $\sigma_\Theta(\gamma, \gamma')$ is the rate of scatterings of electrons from γ to γ' on blackbody photons. Zdziarski (1988) has given an explicit expression for $\sigma_\Theta(\gamma, \gamma')$. The assumption of negligible photon-photon pair production guarantees that collisions between secondary electrons and black body photons take place in the $\epsilon \ll 1$ limit. The total rate of photon injection is then given by $\dot{\phi}_s(\epsilon) + \dot{\phi}_i(\epsilon)$. This photon rate results in a new steady state photon distribution (6), and, in turn, a new secondary electron production rate (11). The production rate of secondary photons resulting from scatterings of the new secondary energetic electrons with the black body photons is calculated and subsequently added to the total rate of photon injection. This procedure is repeated until convergence is achieved (i.e. $\dot{\phi}_s^n + \dot{\phi}_i^n$ for $n = 1, 2, 3, \dots$). For each step the integral equation (6) is solved with the scattering probability (7) numerically by iteration (see e.g. right panel of Fig. 2).

Fig. 3 illustrates the effect of Compton up-scattering of photospheric blackbody photons at $\Theta_\tau \sim 10^{-3} m_e c^2$ by secondary electrons. The dotted curve shows the steady state photon distribution with the inclusion of the soft black-body photons while the black dashed line gives the photon distribution after only the first iteration procedure. The photons from photospheric upscattering dominate the spectrum at $\epsilon \ll 1$. The highest energy (upscattered) photospheric photons are produced by relativistic electrons from Compton downscattering of the primary photons. At lower energies, on the other hand, the upscattered photospheric photons are due to electrons arising from multiple scattered photons. The importance of the upscattered photospheric photons at $\epsilon \leq 0.1$ depends mainly on the low-energy tail distribution of the primary photons and thus its effect on the photon spectra increases with subsequent iterations. This emission could be responsible for the X-ray excess observed in some GRBs. In contrast, at higher energies, the injected photon distribution (i.e. $\dot{\phi}_s^n + \dot{\phi}_i^n$) is not significantly

6 *Ramirez-Ruiz*

alter by subsequent iterations and the role of upscattered photospheric photons to the high-energy spectra can be estimated with only a few iterations.

One does not expect this scattered photospheric component to be a pure Wien spectrum, since in order to change the shape of a soft spectrum and make it into a dilute black body spectrum would require that each photon be scattered $m_e c^2/h\nu$ times by a population of electrons in thermal equilibrium. This requires an optical depth much larger than unity, which is generally not the case anywhere near the photosphere. The scattering depth per shock due to pairs is also unlikely to be much larger, because the scattering and the pair-formation cross sections are comparable, and unless dissipation and pair formation occurs uniformly throughout the entire volume, down-scattering of photons above the pair threshold rapidly leads to self-shielding (Mészáros et al. 2002).

4 DISCUSSION

The standard internal shock model of GRB is generally assumed to produce its observed non thermal radiation by synchrotron (or possibly inverse Compton) process. Here, in addition to synchrotron we have also considered in more detail the role of the outflow photosphere and of possible non thermal distortions in it. A strong baryonic photosphere component should be present at the beginning of bursts. However, the farther beyond the coasting radius the photosphere occurs, the weaker its energy fraction is relative to the primary injected photons arising from internal shocks, because its energy drops as $r^{-3/2}$.

The problem of reprocessing X-rays and γ -rays by Compton scattering could be the key to understanding the X-ray excess above the power-law extrapolation from higher energies observed in a non-negligible fraction of bursts (Kippen et al. 2001; Heise et al. 2001; Amati et al. 2002; Lloyd-Ronning & Ramirez-Ruiz 2002; Sakamoto et al. 2005), although smoothing and softening could be stronger where there is substantial pair formation (Pilla & Loeb 1998; Ghisellini & Celotti 1999; Mészáros et al. 2002; Pe'er & Waxman 2004). If there were a power-law non-thermal spectrum in which significant fraction of the resulting photons are above 1 MeV in the comoving frame, then pair production will change the situation. Photons with a few MeV energies in the comoving frame will then be converted into pairs with very modest γ provided that the compactness parameter is more than unity. The pairs will generally have relativistic energies, and will themselves participate in the synchrotron and inverse Compton emission (Pe'er & Waxman 2004). In reality the actual time dependence for an unsteady outflow leading to shocks, pair formation, and Comptonisation could be more complicated.

If both a photospheric and a shock component are detected, one would expect the thermal photospheric luminosity (and its non thermal part, if present) to vary on similar timescales as the non thermal synchrotron component (unless the shock efficiency is radius dependent, or unless one or both are beyond $r = r_0\eta^2$, in which case $r/(c\eta^2)$ imposes a lower limit on the corresponding variability timescale). The luminosity in a given band (e.g. *Swift*) probably varies differently, since the thermal peak energy is $\propto L^{1/4}$ and falls off steeply, while the synchrotron peak energy varies $L^{3/2}$ and falls off more slowly. A preferred low-energy break (Fig. 3) could be attributed to a scattered photospheric component, provided the baryon loads are low or the outflow variability timescales are large (Fig. 1). This still requires a relatively strong shock synchrotron component, or possibly Alfvén wave Comptonisation in the photosphere (e.g. Thompson 1994), to explain the high-energy power-law spectra. It would also imply a pronounced upward change of slope above the X-ray excess, from the thermal peak to a flatter power law in all bursts where a low break is observed. Further data on X-ray and γ -ray spectral features during the burst (as opposed to the afterglow), will surely offer important clues to the nature of the bulk flow and the macroscopic source of energy driving the microscopic processes of particle acceleration and cooling.

ACKNOWLEDGMENTS

I gratefully acknowledge valuable conversations with P. Mészáros, A. Pe'er, M. J. Rees and E. Waxman. I also thank the referee for helpful correspondence. This work is supported by a Chandra Postdoctoral Fellowship award PF3-40028.

REFERENCES

- Amati L. et al., 2002, *A&A*, 390, 81
- Arons J., 1971, *ApJ*, 164, 437
- Blumenthal G. R., Gould R. J., 1970, *Rev. Mod. Phys.*, 42, 237
- Cavallo G., Rees M. J., 1978, *MNRAS*, 183, 359
- Daigne F., Mochkovitch R., 2002, *MNRAS*, 336, 1271
- Ghisellini G., Celotti A., 1999, *ApJ*, 511, L93
- Goodman J., 1986, *ApJ*, 308, L47
- Heise J. et al., 2001, in *Gamma Ray Bursts in the Afterglow Era*, ed. E. Costa, F. Frontera, and J. Hjorth (Springer: Berlin), 16
- Jauch J. M., Rohrlich F., 1980, *The theory of Photons and Electrons* (Berlin: Springer)
- Kippen R. M. et al., 2001, in *Gamma Ray Bursts in the Afterglow Era*, ed. E. Costa, Frontera F. and Hjorth J. (Springer: Berlin), 22
- Kobayashi S., Ryde F., MacFadyen A., 2002, *ApJ*, 577, 302
- Kompaneets, A. S. 1957, *Soviet Physics - JETP*, 4, 730
- Lloyd-Ronning N. M., Ramirez-Ruiz E., 2002, 576, 101

- Mészáros P., Rees M. J., 2000, *ApJ*, 530, 292
Mészáros P., Ramirez-Ruiz E., Rees M. J., Zhang B., 2002, *ApJ*, 578, 812
Murakami T. et al., 1991, *Nature*, 350, 592
Panaitescu A., Spada M., Mészáros P., 1999, *ApJ*, 522, L10
Pe'er A., Waxman E., 2004, *ApJ*, 613, 448
Pilla R., Loeb A., 1998, *ApJ*, 494, L167
Ramirez-Ruiz E., Merloni A., Rees M. J., 2001, *MNRAS*, 324, 1147
Ramirez-Ruiz E., MacFadyen A. W., Lazzati D., 2002, *MNRAS*, 331, 197
Ramirez-Ruiz E., Lloyd-Ronning N. M., 2002, *NewA*, 7, 197
Rees M.J., Mészáros P., 1994, *ApJ*, 430, L93
Ross R. R., Weaver R., McCray R., 1978, *ApJ*, 219, 292
Sakamoto T. et al., 2005, *ApJ*, 629, 311
Shemi A., Piran T., 1990, *ApJ*, 365, L55
Thompson C., 1994, *MNRAS*, 270, 480
Zdziarski A. A., 1988, *ApJ*, 335, 786